Available online at www.sciencedirect.com
ScienceDirect
Journal of Sound and Vibration 314 (2008) 635–649
JOURNAL OF SOUND AND VIBRATION
www.elsevier.com/locate/jsvi

Vortex sound in unconfined flows: Application to the coupling of a jet-slot oscillator with a resonator

M. Glesser[a,1], V. Valeau[b,*], A. Sakout[a]

[a]*Laboratoire d'Etude des Phénomènes de Transfert Appliqués au Bâtiment, Université de La Rochelle, Av. Michel Crépeau, 17042 La Rochelle cedex 1, France*
[b]*Laboratoire d'Etudes Aérodynamiques, UMR CNRS 6609, 40 Av. du recteur Pineau cedex, 86022 Poitiers cedex, France*

Received 31 July 2007; received in revised form 10 December 2007; accepted 7 January 2008
Handling Editor: C.L. Morfey

Abstract

The aeroacoustical coupling of a jet-slot oscillator to the acoustic resonances of the flow-supply duct is studied in this paper. This configuration, producing self-sustained tones, is original in particular because the source domain is unconfined and the coupling occurs to high-order acoustic resonances. The development of a model, based on the Howe's corollary of the vortex-sound theory permits the flow-acoustic interactions induced in the production of such tones to be modelled theoretically. This model, together with a careful experimental exploration, provided a description of this aeroacoustic sound source. The findings show that the combination of two mechanisms determines the operating frequency that maximizes the acoustic fluctuations responsible for the production of the tones: (i) the energy exchange between the hydrodynamic and the acoustic fluctuations of the fluid, and (ii) the enhancement of the acoustic oscillation by the resonances. Some differences from the usual behaviour of acoustically coupled self-sustained oscillations—in particular, related to the oscillation amplitude and the synchronization between the vortical and acoustical fields—are highlighted.

1. Introduction

Self-sustained tones can be produced when a sheared subsonic flow impinges on a downstream obstacle [1–3]. This type of noise is characterized by an acoustic energy distributed over a few frequency peaks. The establishment of such self-sustained oscillations implies an energy transfer between two fluctuation modes of the gas: (i) the hydrodynamic fluctuations, essentially incompressible, due to the viscosity and describing the flow vorticity, and (ii) the acoustic fluctuations, essentially irrotational and related to flow compressibility [4]. The excitation mechanism is as follows: the sheared flow instabilities are excited at point A of the gas and are amplified during their convection by the mean flow, until vortices are formed. Their impingement on a downstream geometrical singularity, at point B, generates both acoustic (compressible) and hydrodynamic (incompressible) fluctuations. These two consequences of the impingement can interact upstream with the

*Corresponding author.
E-mail addresses: glesser@lma.cnrs-mrs.fr (M. Glesser), vincent.valeau@univ-poitiers.fr (V. Valeau), asakout@univ-lr.fr (A. Sakout).
[1]Present address: CNRS, Laboratoire de Mécanique et d'Acoustique, 31 chemin Joseph Aiguier, 13402 Marseille cedex 20, France.

0022-460X/$ - see front matter
doi:10.1016/j.jsv.2008.01.012

instabilities, near their onset location (point A). If a constructive phase relationship is met along the resulting loop, the feedback controls the increase in instabilities (which can be viewed as a vortex shedding process), inducing an amplification of the gas fluctuations [5–8,2].

If the distance L between A and B is small compared to the emitted-sound wavelength λ_0 ($L \ll \lambda_0$), the velocity fluctuations induced by the hydrodynamic perturbation are dominant at point A. They control vortex shedding and the feedback is called "direct-hydrodynamic". In contrast, if $L \gg \lambda_0$, the acoustic perturbations due to the vortex impingement are dominant at point A and control vortex shedding. The feedback is then called "direct-acoustic" [2].

The previously described sound source can be aeroacoustically coupled with an acoustic resonator. This is the case, for instance, for the closed side branch system [9,10], flue instruments [11,12] or the flow past cavity [13,14]. The relative velocity fluctuations u'/U (u' is the velocity fluctuation and U is the mean flow velocity) induced by the acoustic resonance at the instability onset location was shown to have amplitudes ranging from 10^{-2} to 1 [9,15,10]. These fluctuations control vortex shedding (independently from the distance L), satisfying a Kutta condition [16]. This acoustic coupling imposes the tone frequency and enhances the emitted level. This feedback path is called "indirect-acoustic" in contrast with the upper-mentioned "direct" acoustic or hydrodynamic feedback path. In a recent paper, Rockwell reviewed the models used to determine the dimensionless tones emission frequency for such flow-induced acoustic resonances [17]. Their general form is

$$\frac{f_0 L}{U} = \frac{U_c}{U}(N + a_0), \tag{1}$$

where f_0 is the emission frequency, U_c is the vortice convection speed, N is the oscillation stage and a_0 is an adjustable constant. Eq. (1)-like relations are often called "Rossiter relations" in reference to the author who first introduced them empirically [5].

The present study deals with a geometric configuration called jet-slot oscillator (JSO). It consists of a plane jet impinging on a slotted plate. This configuration has been shown to emit tones that are characterized by high acoustic levels together with a rather complex frequency behaviour. It has been used for flow-control purpose by Ziada [18,19]. In a recent study, Billon et al. [20] showed that the JSO tones, in the particular case where the plane jet is unconfined, can be the result of a direct feedback path (dominant for $Re < 10\,000$, where Re is the jet Reynolds number based on its height H) or of an indirect feedback path due to some aeroacoustical coupling to the flow-supply duct resonances (dominant for $Re > 10\,000$) [21,20]. In this last case, the coupling can occur to high-order acoustic resonances (until order 15th) [22].

The aim of this paper is to study the coupling of the JSO to the acoustic resonances of the flow-supply duct. Experimental and modelling investigations were conducted. An analytical model of the coupling mechanism between the acoustic and the hydrodynamic fluctuations modes, based on the vortex sound theory, has been developed to understand and interpret the complex frequency behaviour of the emitted tones. This model may be seen as "empirical" in the sense that some physical information, which cannot be attained theoretically, is assessed by careful experimental analysis. The vortex sound theory has often been used to model aeroacoustical coupling, but only in the case of confined geometries, and for rather simpler frequency behaviour (coupling to the first two or three acoustic resonances) [11,14,9,23–25]. Some differences with the usual behaviour of acoustically coupled self-sustained tones will also be emphasized.

The paper is organized as follows: after a presentation of the experimental set-up and a description of the flow-acoustic interactions modelling, three aspects are discussed: the influence of coupling on the acoustic fluctuation mode of the gas, the conditions favouring energy transfer from the hydrodynamic fluctuation mode to the acoustic fluctuation mode, and finally, the nature of the feedback.

2. Materials and methods

The experimental set-up described in this section was originally designed to investigate the acoustic phenomena encountered in air-conditioning systems [20].

2.1. Experimental set-up

An airflow, produced by a blower, passes through an expansion volume and a duct ($190 \times 90\,\mathrm{mm}^2$) ending in a nozzle, creating a $H = 10$-mm-high (in the z-direction) and 190-mm-wide plane jet (the duct and the nozzle form what is called the "flow-supply duct" in this paper). The jet impinges on a 4-mm-thick slotted aluminium plate. The plate slot, bevelled at a 45° angle, is aligned with the jet exit and has the same dimensions (Fig. 1). The jet exit/obstacle distance normalized by the jet height H is denoted by L/H and can be moved from 0.5 to 10. The maximum value of the jet velocity at the nozzle exit (denoted by U) can be set from 0 to $27.8\,\mathrm{m\,s}^{-1}$, which corresponds to a Reynolds number based on H ranging from 0 to about 18×10^3.

A 4944-A B&K 1/4″ microphone is mounted behind the obstacle ($x = L + 50$, $y = 85$, $z = 135$, in mm) to measure the radiated tone frequency f_0, i.e. the highest-energy component of the pressure-signal power spectrum.

A Dantec 55R04 hot-wire anemometer is located in the potential core (Fig. 2), in the exit section of the nozzle ($x = 0$), and half-way between the lower and upper edges of the nozzle ($z = H/2$). This part of the jet is not turbulent, so that the main velocity fluctuations ($u_a(t)$) recorded at the tone frequency (f_0) are due to the acoustic velocity generated by the flow-supply duct resonances. This was verified by the measurement of the coherence between this velocity and the resonant pressure field inside the flow-supply duct, which was equal to 0.97 at the emission frequency.

A second Dantec 55R01 hot-wire anemometer is located in the inner sides of the shear layers ($z = 2$ and 8 mm from the lower separation edge, see Fig. 2). Given the rotation of the vortices (clockwise in the lower shear layer and counter-clockwise in the upper one), a probe located at $x = x_0$ measures a maximum x-component perturbation velocity when a vortex passes at x_0. The convection of the successive vortices will thus generate a quasi-sinusoidal fluctuation ($u_h(t)$) at the shedding frequency [26]. While the probe at the nozzle exit measures an acoustic fluctuation $u_a(t)$ at the emission frequency, the probe in the shear layer measures essentially the hydrodynamic fluctuation $u_h(t)$ (at the same frequency, but with a different wavelength) generated by the vortices. The hot-wire is sensitive to both the streamwise velocity fluctuations u_{hx}

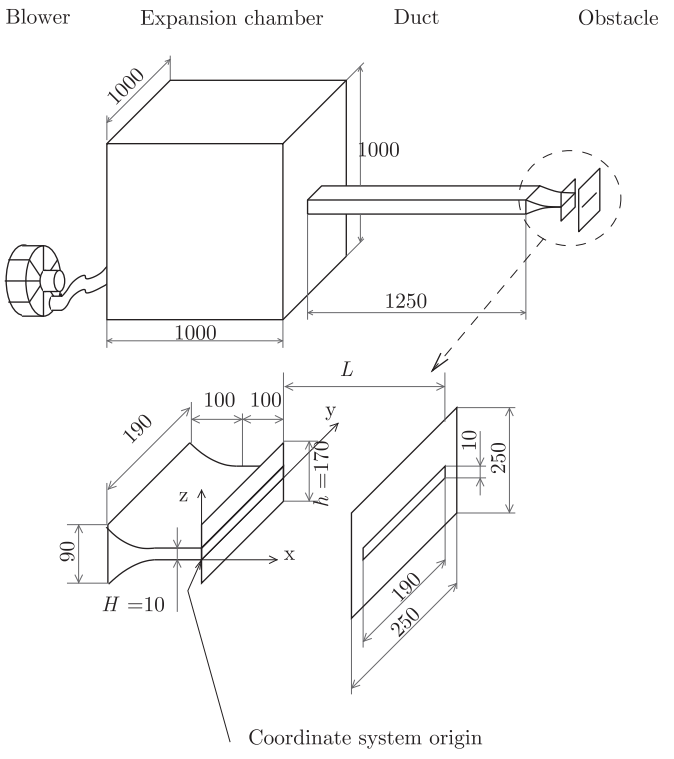

Fig. 1. Overall view of the experimental set-up (dimensions in mm).

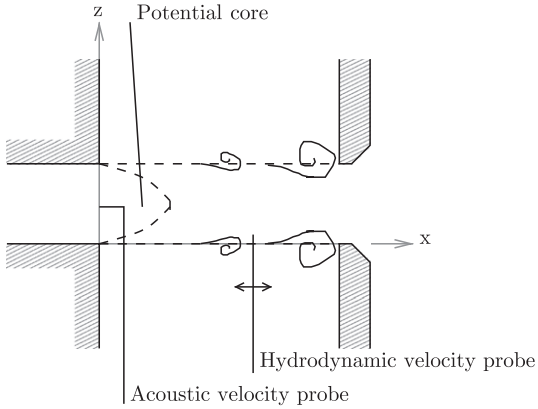

Fig. 2. Velocity probes position.

and the velocity fluctuations normal to the axis of the jet u_{hz}. However, the x-perturbations are superimposed on the mean flow U. The signal $u_h = \sqrt{(U+u_{hx})^2 + (u_{hz})^2}$ measured by the probe is then dominated by the velocity perturbations in the x-direction as long as they remain small compared to the mean flow; indeed, for $u_{hx}/U \ll 1$, the hot-wire reacts linearly to x-perturbations u_{hx} while it reacts quadratically to z-perturbations u_{hz}. The preceding model is then valid in the region near the jet exit where the vortices are not fully developed. It may however fail in the region close to the slot where the vorticity is expected to be concentrated in discrete vortex structures. This may affect, in particular, the hydrodynamic velocity phase measurements (see next paragraph).

For a given jet speed and jet exit/obstacle distance, simultaneous velocity measurements can be carried out with the two probes: the fixed one is located in the potential core of the jet measuring the acoustic velocity, and the mobile one is moved along the jets shear layers, measuring the hydrodynamic velocity. The acoustic velocity will then be used as a phase reference for the hydrodynamic velocity phase estimated experimentally in this study. To estimate the phase between the two measured fluctuations, the cross-spectrum ($S_{ha}(f) = U_h^*(f)U_a(f)$, where $U_h(f)$ and $U_a(f)$ are the Fourier transforms of $u_h(t)$ and $u_a(t)$, respectively) is computed by averaging over 20 segments of a 2048 points signal sampled at 5 kHz. Finally, the phase of the cross-spectrum ($\theta_a - \theta_h$) at the tone frequency f_0 is estimated: it is the phase difference between the resonant acoustic field at the jet exit and the hydrodynamic fluctuation at a given point of the shear layer.

2.2. Preliminary experimental results

The amplitude and frequency of the tones together with the acoustic velocity fluctuations due to resonance were measured for $500 < Re < 18\,000$ and $1 < L/H < 8$. The amplitude of the tones (when coupled to a flow-supply duct acoustic resonance) are plotted as a function of the emission frequency on Fig. 3(a). The corresponding acoustic velocity fluctuations amplitudes are reported on Fig. 3(b). The acoustically coupled source operates at a finite set of emission frequencies up to 1000 Hz, with a notable lack of emission frequencies between 500 and 800 Hz. Beyond 1000 Hz, these emission frequencies are more scattered. The frequency was always lower than 1500 Hz. In all the configurations where self-sustained tones were emitted, the distance L was much smaller than the acoustic wavelength. The amplitude of the tones was generally higher than 80 dB and could reach 115 dB. Finally, the acoustic velocity fluctuations measured at the jet exit were in most cases bounded by the range $10^{-3} < u'/U < 3 \times 10^{-2}$.

The emission frequency can be higher than the cut-off frequency of the duct's first transverse mode in the y-direction, which was found to be 895 Hz. This non-planar mode may then be propagated in the duct; however, its excitation was not confirmed in operating conditions. To assess the nature of the excited acoustic modes, the acoustic phase difference in the y-direction was measured at the tone frequency and at the jet exit ($x = 0$) for different operating conditions (Re, L/H) involving the excitation of the flow-supply duct, by using two hot-wire anemometers placed in the jet potential core (see Fig. 4). Whatever the conditions, the phase

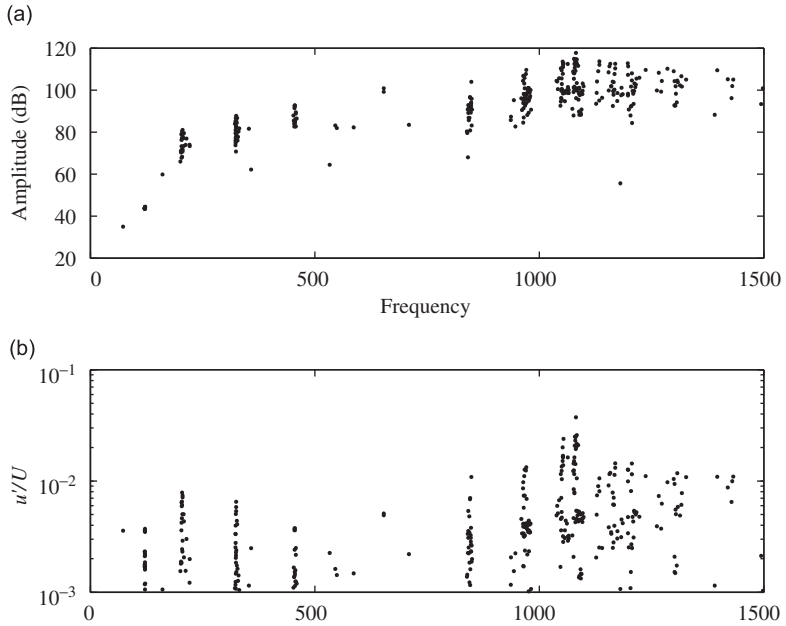

Fig. 3. Tone emission characterization (a) amplitude of the tones in dB (ref. 2×10^{-5} Pa, measured behind the obstacle) and (b) relative acoustic velocity fluctuations at the jet exit (u'/U) as a function of the emission frequency.

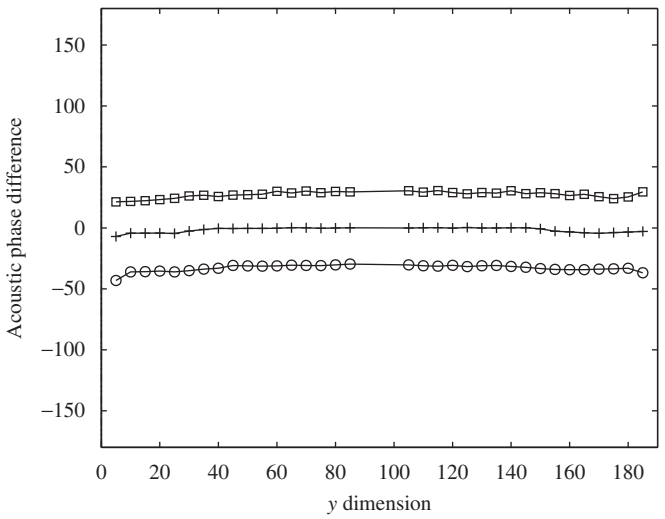

Fig. 4. Acoustic phase pattern at the jet exit: ○ $Re = 16\,000$, $L/H = 3$, $f_0 = 975$ Hz; $+Re = 18\,000$, $L/H = 2,5$, $f_0 = 1215$ Hz; □ $Re = 12\,000$, $L/H = 3$, $f_0 = 975$ Hz. The patterns are, respectively, $-30°$, $0°$ and $30°$-shifted for convenience of interpretation.

pattern was flat. This indicates the propagation of only planar modes at the tone frequency, although the excitation frequency was higher than the first transverse mode cut-off frequency.

3. Flow-acoustic interaction modelling

The development of a flow-acoustic interaction model will be used to identify the conditions favouring energy transfer from the hydrodynamic fluctuation mode to the acoustic fluctuation mode. The development of this model is presented in the following section.

3.1. Existing models

Generally, acoustic fluctuations are one order of magnitude below hydrodynamic fluctuations, and acoustic radiation can be interpreted as an energy dissipation process. The main problem when modelling self-sustained tones is that this acoustic dissipation cannot be ignored in the determination of the flow. Thus at present a three-dimensional (3D) direct numerical simulation is difficult to achieve, particularly for complex geometrical configurations like the JSO. Linearized 3D analytical analyses of the interaction of discrete vortices with an edge or a corner have been proposed by Howe [27]. A relatively simple 2D analytical model was preferred in this study.

An aeroacoustic theory, developed by Powell and Howe [28,11,4] and based on vorticity as a source of sound, can be used to express the acoustic power $\mathscr{P}$ generated in a volume V over one acoustical period T_0 by using the vortical part $\boldsymbol{\omega}$ of the velocity field:

$$\mathscr{P} = \left\langle -\rho_0 \iiint_V (\boldsymbol{\omega} \wedge \mathbf{v}).\mathbf{u}'_a \, \mathrm{d}V \right\rangle_{T_0}, \tag{2}$$

where $\mathbf{v}$ is the velocity field, $\mathbf{u}'_a$ is the acoustic velocity field and $\langle\,\rangle_{T_0}$ denotes an average over one acoustical period. When $\mathscr{P}$ is positive, the hydrodynamic fluctuation mode (related to the vorticity) provides energy to the acoustic fluctuation mode and vice-versa. Flow-excited acoustic resonances have been modelled using this vortex sound theory: flue instruments [11,12], flow past cavities [14,25], pipe sections with closed side branches [9,10,29], whistler nozzles [30] and diaphragms in tandem in a duct [31]. Other applications of this power transfer formula can be found in Ref. [32]. The present section will focus on a model derived from the model of Bruggeman et al. [29,9]. This implementation is considered "semi-empirical", the analytical field models are indeed obtained both from theoretical and experimental investigations (when a theoretical model is not available).

Simplified models of the acoustic field, based on the compact source hypothesis, can be used to obtain this field without having recourse to a full numerical resolution. The acoustic field $\mathbf{u}'_a$ is written, in the complex plane $\tilde{z}$ and in harmonic regime, as a sinusoidal temporal fluctuation $f(t)$ of a potential field [9]:

$$\mathbf{u}'_a = f(t)\boldsymbol{\nabla}(\varphi_{\mathrm{pot}}(\tilde{z})). \tag{3}$$

The scalar field $\varphi_{\mathrm{pot}}(\tilde{z})$ will be called "acoustic-potential field support" in this study. It is obtained by solving the Poisson equation in the studied geometry [16].

The vorticity field is modelled by using the "vortex-point" model initially proposed by Holger [7] and Nelson [14]. This models the vorticity field $\boldsymbol{\omega}$ supposing that the shear layer is rectilinear and the vorticity is only concentrated on discrete vortex-points convected downstream at a constant velocity U_c. The circulation growth of each vortex is evaluated by using the velocity circulation conservation law. It increases linearly:

$$\Gamma_m(t) = UU_c t, \tag{4}$$

until saturation when the following vortex is shed [9], reaching a limit value:

$$\Gamma_{\max} = \frac{UU_c}{f_0}. \tag{5}$$

Modelling the entire vorticity field requires a knowledge of (i) the nature of the jet's oscillation mode (i.e. symmetric or antisymmetric), (ii) the vortice convection speed and (iii) the synchronization with the acoustic fluctuations.

Since vorticity is above zero only in the shear layer, the velocity field $\mathbf{v}$ is modelled, in this zone, by using the relation:

$$\|\mathbf{v}\| = U_c. \tag{6}$$

3.2. Application to the acoustically coupled jet-slot oscillator

The aim of this section is to determine the parameters needed for the development of a 2D model of the flow-acoustic interactions involved in the JSO configuration, in the particular case where the tones are coupled

to the flow-supply duct resonances. The model is not intended to predict the emitted level, but the interaction conditions most favourable to sound emission. The acoustic field was obtained theoretically (Section 3.2.1), and some characteristics of the vorticity field are obtained experimentally (Section 3.2.2).

3.2.1. *Acoustic field modelling*

As the studied domain is compact (see Section 2.2), the acoustic field can be expressed, as stated in the preceding section, as a temporal fluctuation of a potential field. When the acoustic resonance of a flow-supply duct is enhanced, the aeroacoustic source due to the flow-acoustic interactions (located around the obstacle slot) is supposed to be negligible compared to the resonant acoustic source. According to this hypothesis, the acoustic potential field support is mainly induced by the resonator radiation.

The acoustic potential field support is obtained by solving the Poisson equation in a simplified geometry obtained from the actual one by using Schwarz–Christoffel mapping [33]. The geometry bounding the domain under study is a polygon with some vertices placed at infinity (see Fig. 5(a)). Schwarz–Christoffel mapping is then used to compute a transformation of the physical complex plane ($\tilde{z}$-plane) in a canonical complex plane (ζ-plane) where the domain becomes the upper half-plane. The transformation is obtained by using a Schwarz–Christoffel toolbox developed by Driscoll [34]. In the physical plane, the flow-rate emanating from point A_∞ can be considered as a source producing a flow rate $Q = u_{aA}H$ in the domain (u_{aA} being the acoustic velocity at point A). The image of this source in the canonical plane is a point source located in A, producing, in the domain, the flow rate Q over an angle π. As the domain is not confined, the fluid flows out from the physical domain through several points: M_∞, B_∞ and D_∞. Flow-rate sinks of strength $\beta_M Q/\pi$ and $\beta_B Q/\pi$ are then located in M and B, respectively, in the canonical domain, the constant β_M and β_B being for now unknown. The remaining flow rate, which flows out through D_∞ in the physical domain, vanishes at infinity in the canonical domain. The solution of the Poisson equation in the canonical domain is then:

$$\varphi_{\text{pot}}(\zeta) = \frac{Q}{\pi}\ln(\zeta - \xi_A) - \frac{\beta_B Q}{\pi}\ln(\zeta - \xi_B) - \frac{\beta_M Q}{\pi}\ln(\zeta - \xi_M). \tag{7}$$

This solution is calculated in the physical domain by using the inverse Schwarz–Christoffel transformation. In the following, as the emitted level is not predicted, the acoustic flow rate Q is arbitrarily set to one.

In the studied configuration, the main problem of acoustic field determination is the estimation of the parameters β_M and β_B, due to the unconfined geometry. These parameters represent the proportion of fluid flowing out from the domain (i) laterally, between the jet exit and the obstacle, and (ii) through the obstacle, respectively. The determination of the flow-rate distribution is a rather complicated 3D problem. It is evaluated by using a very simplified 2D model based on the unsteady Bernoulli equation, which is verified along streamlines:

$$\rho_0 \frac{\partial \varphi'}{\partial t} + \frac{1}{2}\rho_0 \mathbf{u}^2 + p = K, \tag{8}$$

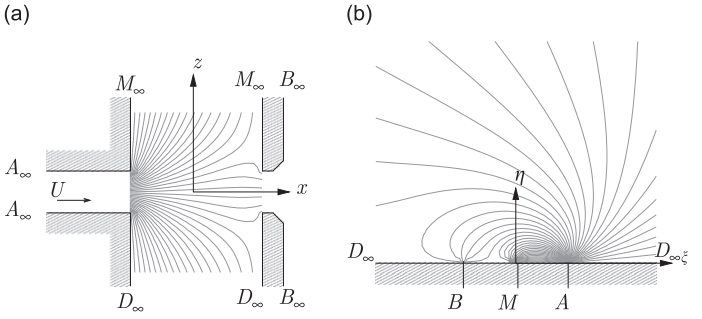

Fig. 5. The geometry under study (a) in the physical plane ($\tilde{z} = x + \mathrm{i}z$) and its image (b) in the canonical plane ($\zeta = \xi + \mathrm{i}\eta$) obtained by Schwarz–Christoffel mapping. The streamlines of the acoustic potential field support are plotted in grey lines (from Eq. (7)).

where K is a real constant value, ρ_0 is the fluid density, p is the pressure, $\mathbf{u} = \mathbf{u}_0 + \mathbf{u}'_a$ is the potential component of the velocity field, where $\mathbf{u}_0$ is the mean potential velocity and $\mathbf{u}'_a$ the acoustic velocity, and $\varphi' = \int \mathbf{u}'_a \, d\mathbf{S}$ is the unsteady scalar velocity potential.

The Bernoulli equation is successively applied along streamlines connecting A_∞ to M_∞ and A_∞ to B_∞. Neglecting the nonlinear terms, conceding some hypotheses based on the flow physics and taking into account flow-rate conservation, a system of equations is obtained. This leads to a rough estimation of the coefficients β_M and β_B, dependent on the emission frequency f_0 through the inertia term $\partial\varphi'/\partial t$ in Eq. (8) (see Appendix A). However, a study of the model sensitivity to the input parameters showed that this flow-rate distribution weakly affects the frequency values optimizing the energy transfer from the hydrodynamic fluctuation mode to the acoustic fluctuation mode (see Appendix A).

3.2.2. *Vorticity field modelling*

Fig. 6 depicts, for $Re = 11\,800$ and $L/H = 3.3$, the cross-spectrum phase (see Section 2.1) as a function of the mobile probe location in the upper ($z = 8$ mm) and lower ($z = 2$ mm) shear layers. The phase variation is linear and nearly identical for both shear layers. This behaviour was observed for other values of Re and L/H corresponding to indirect feedback paths and allowed us to focus only on one shear layer in the following experiments. The linearity of the phase variation in the region close to the slot suggests that the hot-wire response to normal velocity perturbation (Section 2.1) did not affect the hydrodynamic phase measurements. The cross-spectrum phase is also plotted as a function of the mobile probe location in the upper shear layer, for different pairs (Re, L/H) corresponding to different tone frequencies (between 322 and 1285 Hz, see Fig. 7).

Fig. 6 shows that the upper and lower vortices are convected symmetrically at the same constant convection speed (linear phase variation), from the jet exit to the impingement location. The jet mode is then symmetric.

In addition, the phase difference of the hydrodynamic velocity between two successive positions x_1 and x_2 of the mobile probe (with $x_2 - x_1 = \Delta x$) can be related to the time ($t_c = \Delta\theta/2\pi f_0$) needed by the vortex to travel the distance Δx. The slope of the straight line $\Delta\theta(x)$ can then be related to the mean convection speed of the structures between x_1 and x_2: $U_c = 2\pi f_0(\Delta\theta/\Delta x)^{-1}$. Figs. 6 and 7 can then be used to estimate the value $U_c/U = 0.6$ (with a precision of about $\pm 3\%$). This result is in agreement with the values found in the literature [2], and validates the idea that the probe located in the shear layer measures essentially a hydrodynamic fluctuation (if it measured an acoustic fluctuation, the phase velocity obtained would correspond to the speed of sound).

Knowing the phase of the acoustic cycle at which the vortices are shed is crucial for the development of a flow-acoustic interaction model. This phase can be deduced from the experimental data and needs to be

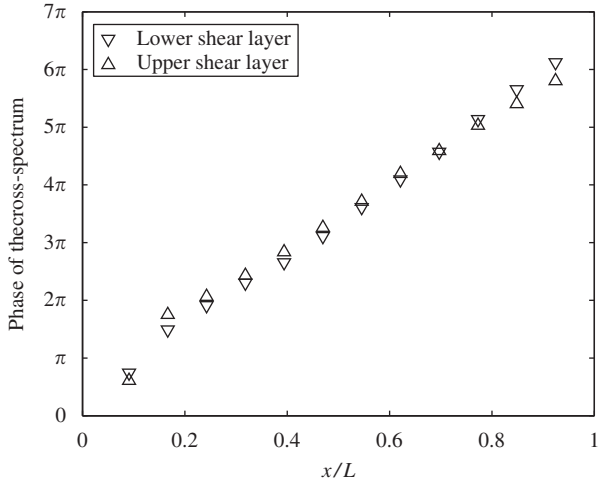

Fig. 6. Cross-spectrum phase versus mobile probe location ($Re = 11\,800$, $L/H = 3.3$, $f_0 = 962$ Hz).

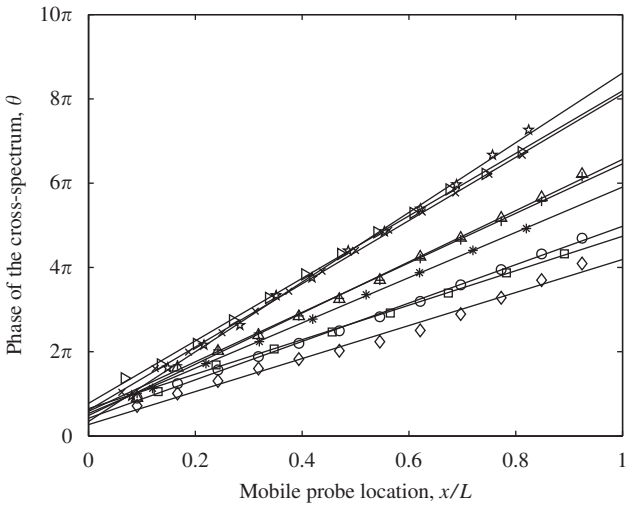

Fig. 7. Cross-spectrum phase as a function of the mobile probe location. The solid lines correspond to a linear regression of the experimental data. ⋆ $Re = 11\,800$, $L/H = 3,7$, $f_0 = 1175$ Hz; ▷ $Re = 8240$, $L/H = 3,7$, $f_0 = 960$ Hz; × $Re = 11\,800$, $L/H = 4$, $f_0 = 1285$ Hz; △ $Re = 11\,800$, $L/H = 3,3$, $f_0 = 962$ Hz; + $Re = 15\,000$, $L/H = 3,3$, $f_0 = 1187$ Hz; ∗ $Re = 11\,800$, $L/H = 2,5$, $f_0 = 1182$ Hz; ○ $Re = 18\,051$, $L/H = 3,3$, $f_0 = 1064$ Hz; □ $Re = 11\,800$, $L/H = 2,3$, $f_0 = 957$ Hz; ◇ $Re = 6429$, $L/H = 3,3$, $f_0 = 322$ Hz.

carefully assessed, as the results given by the theory of Powell and Howe (Eq. (2)) are highly sensitive to the synchronization between the acoustic and vortical fields. A straightforward experiment would be to measure simultaneously the acoustic velocity (at $x = 0$ and $z = H/2$) and the hydrodynamic velocity in the shear layer at the shedding point ($x = 0$ and $z = 0$ or H); however, at this location, it is difficult to assess precisely which type of velocity (acoustic or hydrodynamic) is actually measured. The method would then be highly questionable. The cross-spectrum phase at vortex shedding (at $x = 0$) is then extrapolated from the linear variation of the phase curves plotted in Fig. 7, measured for $0.05 < x/L < 0.9$ (supposing that this variation remains linear very close to $x = 0$). Remembering that all phases are referenced with respect to the acoustic fluctuation at the nozzle exit (Section 2.1), the extrapolated value at $x = 0$ is an estimation of the phase difference between the acoustic and hydrodynamic fluctuations at vortex shedding, and can be used to synchronize the acoustic and vorticity fields of the theoretical model. For every configuration in Fig. 7, the acoustic phase at vortex shedding is close to $\pi/2$ (with a maximal deviation of $\pm 0.3\pi$).

The physical interpretation of this result is the following: a vortex is supposed to be shed, at the jet exit, at $t = 0$. As explained in Section 2.1, this vortex generates a maximum of the velocity fluctuation because it is measured at the inner side of the jet. The corresponding hydrodynamic velocity fluctuations can then be written as follows: $u_h(t) = \cos(2\pi f_0 t)$. The phase θ_h is then null ($\theta_h = 0$). The measurements give $\theta_a - \theta_h = \pi/2$ (Section 2.1), that is $\theta_a = \pi/2$. The acoustic velocity, $u_a(t) = \cos(2\pi f_0 t + \pi/2)$ is then zero and turns upstream (i.e. negative) at the instant of vortex shedding. In other words, a new vortex is shed each time the particles located at the open end of the nozzle are stopped at the end of their downstream acoustic displacement and start to return upstream in the opposite direction to the mean fluid motion. This result is in contradiction with those observed at the exit of the whistler nozzle [30], or at the neck of a cavity acoustically coupled to a grazing flow [14,35].

Taking into account the experimental results, the vorticity field can be modelled as described in Section 3.1. The vorticity is only concentrated in point vortices convected from the jet exit to the obstacle on a rectilinear path, symmetrically, in each shear layer and at the speed $U_c = 0.6U$. A vortex is shed in each shear layer when the phase of the co-sinusoidal acoustic field is equal to $\pi/2$. Vorticity ejected to the right of the aperture plate was not taken into account. Additional measurements showed that no coherent structures can be identified in this area. This can therefore be considered as a second-order effect that would not significantly alter the resonances of the system.

3.2.3. Model implementation

Finally, the flow-acoustic interaction model was computed by using Eq. (2) with the field models described previously. The model admits as input variables:

- the flow velocity U (or a Reynolds number Re),
- the distance from the jet exit (nozzle end) to the obstacle L,
- the emitted frequency f_0,
- the acoustic velocity at the jet exit.

In addition, some terms are set empirically for field modelling:

- the vortices convection speed,
- the phase of the acoustic cycle corresponding to vortex shedding,
- the jet oscillation mode.

The model implemented can be used to evaluate the acoustic power $\mathscr{P}$ generated or absorbed by the energy transfer between the hydrodynamic fluctuation mode and the acoustic fluctuation mode of the gas.

4. Discussion

4.1. Influence of coupling on the acoustic oscillation frequencies

When the tones are acoustically coupled to the flow-supply duct resonances, the amplitude of the acoustic fluctuations depends on the resonance efficiency of the duct. The flow-supply duct is excited by the aeroacoustic source at the open end of the nozzle. The efficiency of the response of the resonator (and thus the amplitude of the acoustic fluctuations) is then directly proportional to its input admittance (at the open end section).

In spite of the relatively high emission frequency (see Fig. 3), the first transverse mode was not propagated in the flow-supply duct (see Section 2.2). The calculation of the longitudinal plane mode admittance is then sufficient to characterize the duct resonance. This was performed on a 2D equivalent duct by using a conventional decomposition in a succession of elementary ducts of constant cross sections. Each elementary duct was modelled by an acoustic transfer matrix taking into account the propagation of plane waves with visco-thermic losses at the duct wall. The reduced duct input admittance (ratio between the admittance at the nozzle exit and the characteristic admittance of the air: $Y_c = 1/\rho_0 c$, c being the sound velocity) was finally calculated by multiplying together the obtained matrices (see Fig. 8(a)). The admittance of the nozzle only was also plotted in Fig. 8(a) in order to assess its influence on the flow-supply duct response. The tone emission frequencies measured for a large set of pairs (Re, L/H) are shown in Fig. 8(b).

The emission frequencies selected by the aeroacoustic source correspond to the resonant frequencies of the duct (i.e., to the frequencies where the input admittance is maximum). The effect of the nozzle on duct admittance explains the lack of tones between 500 and 800 Hz. Indeed, nozzle admittance was at a minimum around 600 Hz, involving a reduction of the duct admittance around this frequency and acting as a filter in the frequency range [500–800] Hz. The efficiency of the resonance is not then sufficient to maintain an indirect feedback path. Moreover, nozzle admittance was at a maximum around 1100 Hz. This causes a widening and an amplification of the flow-supply duct admittance peaks. The indirect feedback path can then be maintained for an emission frequency diverging from the resonant frequency: this could explain the dispersion of the measured emission frequencies beyond 1000 Hz.

As a conclusion, when coupled with the resonator, the acoustic fluctuations (responsible for tone production) are enhanced by the acoustic energy provided by the resonance. The coupling therefore imposes an *acoustic constraint* on the emission frequency selection, in order to maximize these acoustic fluctuations.

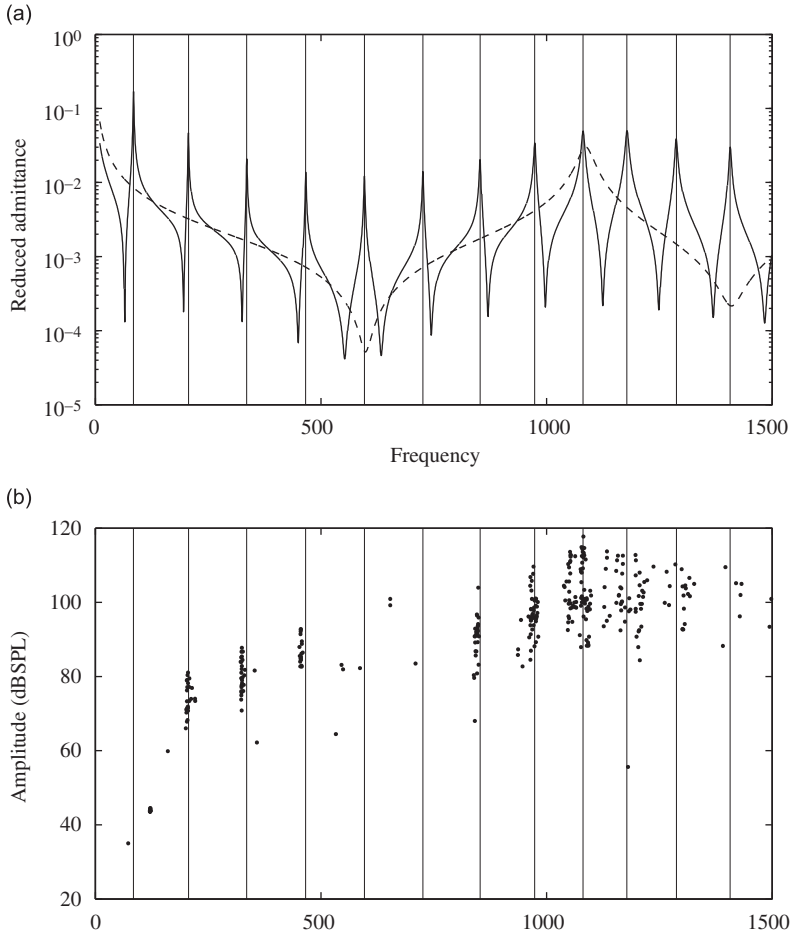

Fig. 8. Comparison between (a) the input admittance of — the flow-supply duct, - - - the nozzle and (b) the tone sound pressure level (measured behind the obstacle) as a function of the frequency.

4.2. Energy transfer between the hydrodynamic and acoustic fluctuations

The power $\mathscr{P}$ generated by the energy transfer between the hydrodynamic and the acoustic fluctuations of the gas was calculated for a given Reynolds number, for variable emission frequencies and variable jet-exit/obstacle distances, by using the model described in Section 3. The distribution of the power produced as a function of L/H and f_0 was obtained for $Re = 11\,800$ and $16\,000$, two Reynolds numbers ensuring a flow-supply duct resonance (Fig. 9). The emission frequencies measured for these Reynolds numbers are superimposed on the plots. This behaviour is typical of flow-excited acoustic resonances. As the distance L was increased, the tone frequency decreased, describing a hyperbole; the frequency jumps corresponding to the transition from one oscillation stage to another [2]. For each oscillation stage, the tone frequency depicts steps at almost constant frequency. These step frequencies correspond to the resonant frequencies of the flow-supply duct (represented by dashed lines) as underlined in the previous section.

The emission frequencies "chosen" by the system for a given pair $(Re, L/H)$ correspond closely, in the plane $(L/H, f_0)$, to the hyperbole-shaped zones of maximum positive power predicted by the model. In these zones, the energy transfer from the hydrodynamic to the acoustic fluctuations was maximal (i.e. the power $\mathscr{P}$ was maximal). It is noticeable that these zones are very accurately predicted by the Rossiter relation (Eq. (1)) with $a_0 = -1/8$ (relation represented as a solid line in Fig. 9). The agreement between the vortex-sound theory and

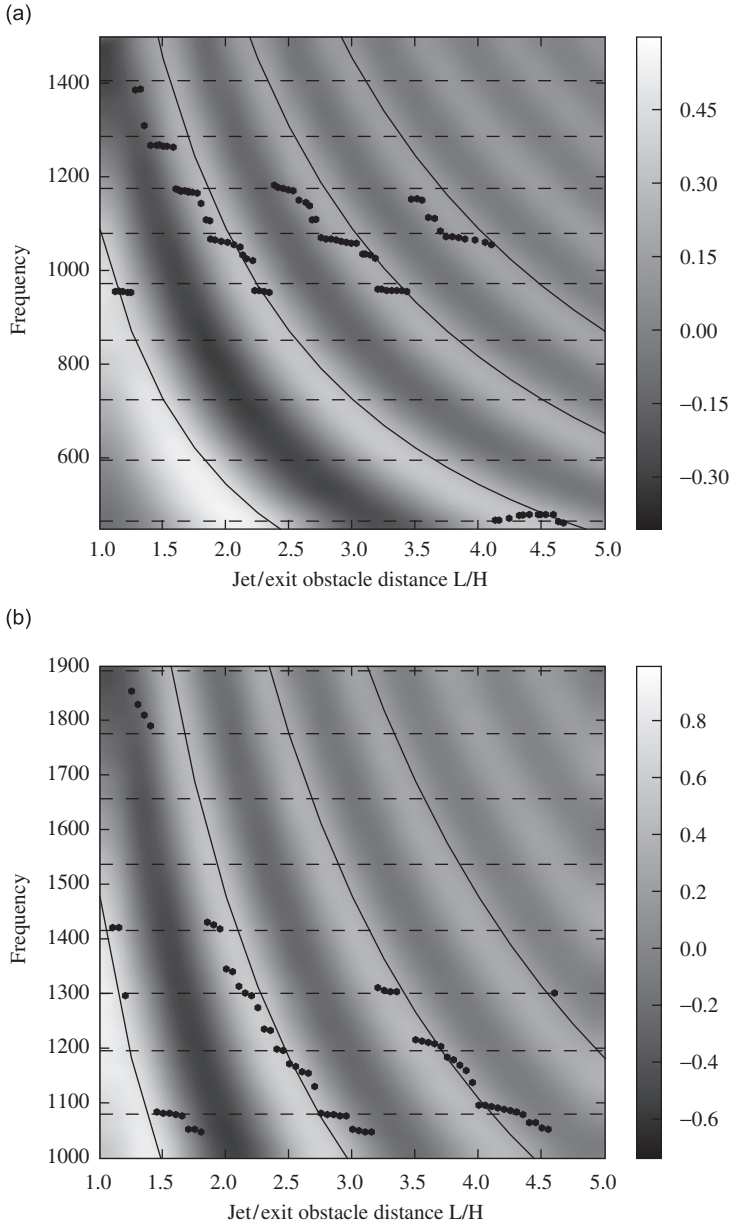

Fig. 9. Distribution of the power $\mathscr{P}$ generated by the flow-acoustic interactions calculated for variable emission frequencies and variable jet-exit /obstacle distance: (a) $Re = 11\,800$ and (b) $Re = 16\,000$. • tone frequencies measured for different values of L/H, - - - duct resonant frequencies, — frequencies predicted by the Rossiter equation (Eq. (1)).

the Rossiter relation, obtained theoretically by decomposing the feedback loop, must be underlined. The maximization of the energy transfer from the hydrodynamic to the acoustic fluctuations imposes a further constraint called *hydrodynamic constraint* on the emission frequency selection.

Finally, two mechanisms maximizing the energy transfer to the acoustic fluctuation mode together set the emission frequency; the energy is provided (i) by the resonance (ii) by the coupling to the hydrodynamic fluctuations. These optimal conditions correspond, in the $(L/H, f_0)$ plane, to the intersection between the horizontal lines (representing the acoustic constraint) and the Rossiter hyperboles (representing the hydrodynamic constraint), as shown in Fig. 9.

4.3. Nature of the indirect feedback

As recalled in the introduction section, in the case of the flow-acoustic resonances described in the literature, vortex shedding is controlled by the acoustic velocity induced by the resonance. In this case, a new vortex is shed at the nozzle lips when the acoustic velocity is zero and turns towards the exit of the duct (satisfying a Kutta condition as the velocity induced at the edge by the vorticity compensates for the singularity of the potential flow which would exist in the absence of vorticity [16]). The feedback is then purely acoustic.

In the case of the JSO, the experimental observations seem to accredit a different feedback scenario. Firstly, a new vortex is shed each time the acoustic velocity due to resonance is zero and turns upstream, which is in contradiction with a Kutta condition if this acoustic velocity controls shedding. Secondly, the amplitude of the acoustic fluctuations measured at the nozzle exit ($10^{-3} < u'/U < 3 \times 10^{-2}$) are at least one order of magnitude below the fluctuation levels reported in the literature for other configurations ($10^{-2} < u'/U < 1$). These observations may indicate that the acoustic oscillations due to the resonance are not dominant at the nozzle lips, in contrast to the hydrodynamic oscillations induced by the vortex convection. This assumption seems to be confirmed by an estimation of the hydrodynamic velocity induced at the nozzle lips by a single-impinging vortex, using Eq. (5) describing the maximum vortex circulation and the Biot–Savart's law [16]:

$$\frac{u'_h}{U} = \frac{\Gamma_{\max}}{2\pi L U} = \frac{U_c}{2\pi f_0 L}. \tag{9}$$

For example, in the configuration used in Fig. 6 ($Re = 11\,800$, $U = 18\,\mathrm{m\,s^{-1}}$, $L/H = 3.3$, $f_0 = 962\,\mathrm{Hz}$), the ratio u'_h/U is close to 5×10^{-2}. As a consequence, the hydrodynamic fluctuations induced by the vortex convection seem to be at least of the same order of magnitude as the acoustic fluctuations due to the resonance. The feedback could then be hydrodynamic.

However, the hypothesis of a hydrodynamic feedback fails to explain the emission frequency lock-in by the acoustic resonance, clearly illustrated by the steps at almost constant frequency in Fig. 9. In summary, two phenomena seem to be in competition for the control of vortex shedding. The studied case probably lies "in-between" purely hydrodynamic feedback and purely acoustic feedback.

5. Conclusion

Under certain geometrical conditions, the tones produced by an unconfined jet-slot oscillator (JSO) can be coupled to the acoustic resonances of the flow-supply duct. The development of a model based on the Howe's corollary of the vortex-sound theory can be used to model theoretically the flow-acoustic interactions induced in tones production. This model, together with a careful experimental exploration, enable a description of the acoustically coupled JSO.

The acoustic fluctuations responsible for tone production are initiated by the *aeroacoustic energy exchange* with the hydrodynamic fluctuations. These acoustic fluctuations are enhanced by the *acoustic energy due to the resonance*. These two mechanisms together set the operating frequency which maximizes the acoustic fluctuations. The coupling imposes an acoustic constraint in order to maximize the acoustic resonance efficiency. The maximization of energy transfer from the hydrodynamic to the acoustic fluctutation mode imposes a hydrodynamic constraint predicted either by a vortex sound theory-based model or by a Rossiter-like relation. It is noteworthy that a general flow-acoustic interaction model (such as the one based on vortex sound theory) predicts the same critical Strouhal numbers for whistling as a Rossiter-like relation, often obtained by using the feedback loop stability theory.

The acoustically coupled JSO is an original configuration where the limit between acoustic and hydrodynamic feedback does not seem to be clearly defined. It has both the physical features of systems controlled by acoustic feedback and an unusual synchronization between the acoustic field and vortex shedding for such systems. No firm conclusion can be drawn as to whether vortex shedding is controlled by the acoustic velocity fluctuations due to resonance or by hydrodynamic velocity

fluctuations generated by vortex convection. The system could thus be intermediate between a flute and an edge-tone.

Acknowledgements

The authors wish to thank Prof. A. Hirschberg for some valuable discussions about flow-acoustic interaction modelling (especially on the acoustic flow-rate distribution model) and Prof. J.P. Dalmont for providing the routines used to calculate duct input admittance.

Appendix A. Acoustic flow distribution

The acoustic flow-rate distribution determination is a rather complicated problem. A rough estimation of this distribution is achieved by using the unsteady Bernoulli equation (Eq. (8)), supposing a quasi-steady fluid behaviour in the slot region and a dominance of the inertia in the lateral region. This model is limited to the case where the distance L is small compared to the lateral branch length. It leads to the following solutions (see Ref. [36] for detailed calculation):

$$\beta_M = \frac{u_{aM}}{u_{aA}} = \frac{\omega HL(\omega L^2 + \omega hH/2) + \mathrm{j}\omega HL^2 U}{L^2U^2 + (\omega L^2 + \omega hH/2)^2},$$
$$\beta_B = \frac{u_{aB}}{u_{aA}} = \frac{L^2U^2 - \omega hH/2(-\omega L^2 - \omega hH/2) - \mathrm{j}\omega L^3 U}{L^2U^2 + (\omega L^2 + \omega hH/2)^2}, \tag{A.1}$$

the length h being defined in Fig. 1, and ω being the acoustic pulsation.

The consequence of an eventual estimation error on the preceding results was then studied. For this purpose, the acoustic power $\mathscr{P}$ was simulated as a function of the frequency for a given pair (Re, L/H) and for different acoustic flow-rate distributions (Fig. 10). The different distributions were obtained by varying the flow rate through the obstacle with respect to that obtained theoretically (Eq. (A.1)). The frequency values maximizing the power $\mathscr{P}$ were weakly affected, the variation of the flow-rate distribution influencing mostly the amplitude. This result confirms that the flow-rate distribution has a weak effect on the position of the frequencies maximizing the energy transfer from the hydrodynamic to the acoustic fluctuation.

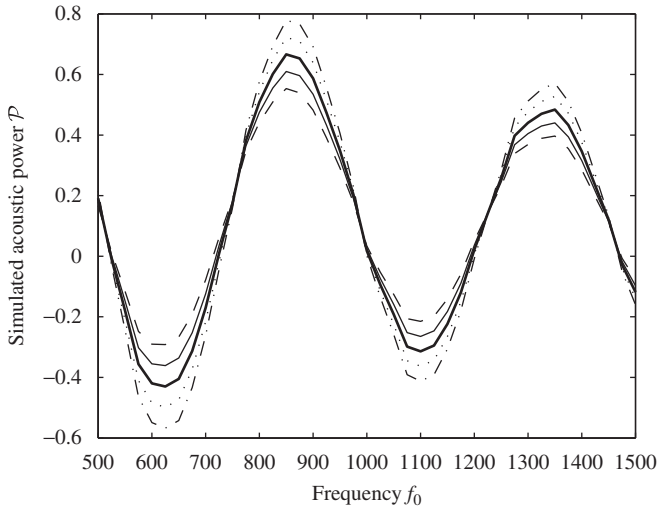

Fig. 10. Power $\mathscr{P}$ simulated as a function of the emission frequency ($Re = 15000$, $L/H = 3$), influence of the acoustic flow-rate distribution: *bold solid line* estimated distribution (equation (A.1)), *solid line* −10% through the obstacle, ⋯ +10% through the obstacle, – – −20% through the obstacle, – · – +20% through the obstacle.

References

[1] J.W.S. Rayleigh, *The Theory of Sound*, Vol. 2, Dover, New York, 1945.
[2] W.K. Blake, A. Powell, The development of contemporary views of flow-tone generation, *Recent Advances in Aeroacoustics*, Springer, New York, 1986, pp. 247–325.
[3] A. Powell, Some aspects of aeroacoustics: from Rayleigh until today, *Journal of Vibration and Acoustics* 112 (1990) 145–159.
[4] M.S. Howe, The dissipation of sound at an edge, *Journal of Sound and Vibration* 70 (3) (1980) 407–411.
[5] J.E. Rossiter, Wind tunnel experiments on the flow-over rectangular cavities at subsonic and transonic speeds, Technical Report 64037, Royal Aircraft Establishment, 1964.
[6] R.C. Chanaud, A. Powell, Some experiments concerning the hole and ring tone, *Journal of the Acoustical Society of America* 37 (5) (1965) 902–911.
[7] D.K. Holger, T.A. Wilson, G.S. Beavers, Fluid mechanics of the edgetone, *Journal of the Acoustical Society of America* 62 (5) (1977) 1116–1128.
[8] D. Rockwell, E. Naudascher, Self-sustained oscillations of impinging free shear layers, *Annual Review of Fluid Mechanics* 11 (1979) 67–94.
[9] J.C. Bruggeman, A. Hirschberg, M.E.H. van Dongen, A.P.J. Wijnands, J. Gorter, Flow induced pulsations in gas transport system: analysis of the influence of closed side branches, *Journal of Fluids Engineering* 111 (1989) 484–491.
[10] S. Dequand, S.J. Hulshoff, A. Hirschberg, Self-sustained oscillations in a closed side branch system, *Journal of Sound and Vibration* 265 (2) (2003) 359–386.
[11] M.S. Howe, Contributions to the theory of aerodynamic sound, with application to excess jet noise and the theory of the flute, *Journal of Fluid Mechanics* 71 (4) (1975) 625–673.
[12] S. Dequand, J.F.H. Willems, M. Leroux, R. Vullings, M. Van Weert, C. Thieulot, A. Hirschberg, Simplified models of flue instruments: influence of mouth geometry on the sound source, *Journal of the Acoustical Society of America* 113 (3) (2003) 1724–1735.
[13] L.L. Shaw, Suppression of aerodynamically induced cavity pressure oscillations, *Journal of the Acoustical Society of America* 66 (3) (1979) 880–884.
[14] P.A. Nelson, N.A. Halliwell, P.E. Doak, Fluid dynamics of a flow excited resonance, part 2: flow acoustic interaction, *Journal of Sound and Vibration* 91 (3) (1983) 375–402.
[15] P.C. Kriesels, M.C.A.M. Peters, A. Hirschberg, A.P.J. Wijnands, A. Iafrati, G. Riccardi, R. Piva, J.C. Bruggeman, High amplitude vortex-induced pulsation in a gas transport system, *Journal of Sound and Vibration* 184 (2) (1995) 343–368.
[16] S.W. Rienstra, A. Hirschberg, *An Introduction to Acoustics*, Vol. IWDE 01-03, Eindhoven University of Technology, 2003.
[17] D. Rockwell, J.-C. Lin, P. Oshkai, M. Reiss, M. Pollack, Shallow cavity flow tone experiments: onset of locked-on states, *Journal of Fluids and Structures* 17 (3) (2003) 381–414.
[18] S. Ziada, Feedback control of globally unstable flows: impinging shear flows, *Journal of Fluids and Structures* 9 (8) (1995) 907–923.
[19] S. Ziada, Interaction of a jet-slot oscillator with a deep cavity resonator and its control, *Journal of Fluids and Structures* 15 (6) (2001) 831–843.
[20] A. Billon, V. Valeau, A. Sakout, Two feedback paths for a jet-slot oscillator, *Journal of Fluids and Structures* 21 (2005) 121–132.
[21] A. Billon, V. Valeau, A. Sakout, Flow instabilities producing the slot-tone, *Comptes Rendus de l'Académie des Sciences—Series IIB—Mechanics* 332 (7) (2004) 557–563.
[22] M. Glesser, A. Billon, V. Valeau, A. Sakout, Influence of the resonator damping on its coupling with a jet-slot oscillator, *Twelfth International Congress on Sound and Vibration*, Lisbon, Portugal, 2005.
[23] S. Dequand, X. Luo, J. Willems, A. Hirschberg, Helmholtz-like resonator self-sustained oscillations, part 1: acoustical measurements and analytical models, *AIAA Journal* 41 (3) (2003) 408–415.
[24] S. Dequand, S. Hulshoff, H. van Kuijk, J. Willems, A. Hirschberg, Helmholtz-like resonator self-sustained oscillations, part 2: detailed flow measurements and numerical simulations, *AIAA Journal* 41 (3) (2003) 416–423.
[25] M. Meissner, Aerodynamically excited acoustic oscillations in cavity resonator exposed to an air jet, *Acta Acustica united with Acustica* 88 (2002) 170–180.
[26] P.A. Nelson, N.A. Halliwell, P.E. Doak, Fluid dynamics of a flow excited resonance, part 1: experiment, *Journal of Sound and Vibration* 78 (1) (1981) 15–38.
[27] M.S. Howe, Edge, cavity and aperture tones at very low mach numbers, *Journal of Fluid Mechanics* 330 (1997) 61–84.
[28] A. Powell, Theory of vortex sound, *Journal of the Acoustical Society of America* 36 (1) (1964) 177–195.
[29] J.C. Bruggeman, Flow Induced Pulsations in Pipe Systems, PhD Thesis, Technische Universiteit Eindhoven, Eindhoven, 1987.
[30] A. Hirschberg, J.C. Bruggeman, A.P.J. Wijnands, N. Smits, The "whistler nozzle" and horn as aero-acoustic sound sources in pipe systems, *Acustica* 68 (1989) 157–160.
[31] K. Hourigan, M.C. Welsh, M.C. Thompson, A.N. Stokes, Aerodynamic sources of acoustic resonance in a duct with baffles, *Journal of Fluids and Structures* 4 (1990) 345–370.
[32] M.S. Howe, *Acoustics of Fluid–Structure Interactions*, Cambridge University Press, Cambridge, 1998.
[33] L.M. Milne-Thomson, Theorem of Schwarz and Christoffel, *Theoretical Hydrodynamics*, Macmillan Co., London, 1968 (Chapter X).
[34] T.A. Driscoll, A matlab toolbox for Schwarz–Christoffel mapping, *ACM Transactions on Mathematical Software* 22 (2) (1996) 168–186.
[35] P.M. Radavitch, S. Ahmet, J. Novak, A computational approach for flow-acoustic coupling in closed side branches, *Journal of the Acoustical Society of America* 109 (4) (2001) 1343–1353.
[36] M. Glesser, Sons auto-entretenus produits par l'interaction d'un jet plan avec une plaque fendue: étude expérimentale et modélisation du couplage avec un résonateur, PhD Thesis, Université de La Rochelle, 2006.